Journal of Asian Earth Sciences 263 (2024) 106033

Contents lists available at ScienceDirect

Journal of Asian Earth Sciences

journal homepage: www.elsevier.com/locate/jseaes

# Orbital cycles recorded in Early Cambrian shales with implications for organic matter accumulation

Siding Jin [a,b], Yan Liu [a,b,*], Chao Ma [b,c], Quanlin Zhang [d], Anqing Chen [b,c]

[a] College of Energy, Chengdu University of Technology, Chengdu 610059, China
[b] State Key Laboratory of Oil and Gas Reservoir Geology and Exploitation, Chengdu University of Technology, Chengdu 610059, China
[c] Institute of Sediment. Geol., Chengdu University of Technology, Chengdu 610059, China
[d] Southwest Oil & Gas Company, SINOPEC, Sichuan 610041, China

ARTICLE INFO

*Keywords:*
Orbital timescale
Eccentricity pacing
Shales
Astronomical calculations
Bio-evolution

ABSTRACT

The Qiongzhusi Formation, dating back to the Early Cambrian period and located in the Yangtze Block of the South China Craton, is distinguished by its organic-rich shales. These shales, which developed during the pivotal "Second Cambrian Explosion" have increasingly become a focal point of scholarly research. Previous studies have identified a stratigraphic transition in Qiongzhusi Formation, signaling a major shift in the Early Cambrian ocean-climate system. While existing geochemical analyses have shed light on primary productivity and redox conditions, the impact of orbital-forcing on organic matter accumulation remains poorly understood. This study reports on the results of iron to aluminum ratio (Fe/Al) and total organic carbon (TOC) assessments conducted on Early Cambrian shale samples from drill hole JS103 in the Sichuan Basin. The analysis spans approximately 10.8 million years, covering Stages 2–3 (from ~526 Ma to ~515 Ma), and is based on data derived from astronomical tuning. Our findings reveal hierarchal periodicities corresponding to 405, ~100 and ~36-kyr cycles. Notably, the observed phase shifts in the 405-kyr filtered Fe/Al and TOC data series around ~521 Ma indicate potential orbitally driven variations in carbon cycling, possibly influencing monsoon dynamics. Higher Fe/Al ratios indicate enhanced preservation under anoxia environmental conditions, while low ratios alongside high TOC suggest increased productivity due to nutrient influx. The phase shifts observed in the coupled series on a 405-kyr cycle scale imply a significant transformation of the ocean-climate system, driven by strong eccentricity pacing during the "second Cambrian explosion". This suggests that Cambrian biotic radiation could have been influenced by astronomical forcing and variations in oceanic oxygen levels.

## 1. Introduction

The burial and accumulation of organic matter are crucial processes in the genesis of petroleum resources (Bjørlykke, 2010; Tyson, 2001) and these complex geological processes serve as key components of global carbon budget (Berner, 1990; Hesselbo et al., 2003; Canuel et al., 2012; Wang et al., 2022). These processes, especially within sedimentary environments, are profoundly influenced by environmental conditions that govern preservation or productivity (Stow et al., 2001). Key factors impacting organic matter accumulation include vegetation coverage (Jones and Manning, 1994), precipitation and runoff (Bosmans et al., 2020), redox conditions (Lu et al., 2021), and hydrologic cycle (Wang et al., 2020), all modulated by insolation and climate change. Studies indicate that Earth's orbital parameters significantly influence climate change variations and consequentially organic matter accumulation. For instance, Eldrett et al. (2015) assumed that reduced obliquity and eccentricity correlate with enhanced organic matter preservation due to stable water stratification and expanded minimum oxygen zones. Charbonnier et al. (2018) detected a strong obliquity signal during OAE2, linked to accelerated organic matter accumulation. Similarly, Huang et al. (2021) reported an astronomical rhythm in deep-time organic matter burial, establishing a model for obliquity-forced accumulation. The role of precession in eccentricity modulation, as demonstrated by Herrle et al. (2003) and Winguth et al. (2013), highlights the monsoon's influence on nutrient availability and carbon burial rates, further supported by the work of Benamara et al. (2020).

In the context of Qiongzhusi Formation, widely distributed across South China's Upper Yangtze Platform (Jin et al., 2016), and the source

* Corresponding author at: College of Energy, Chengdu University of Technology, Chengdu 610059, China.
*E-mail address:* liuyan08@cdut.cn (Y. Liu).

https://doi.org/10.1016/j.jseaes.2024.106033
Received 16 April 2023; Received in revised form 11 January 2024; Accepted 25 January 2024
Available online 1 February 2024

of major Cambrian gas reservoirs in the Sichuan Basin (Zou et al., 2014), understanding the organic matter accumulation mechanisms becomes critical. Despite significant gas outputs from exploration well like JS103HF, the organic accumulation mechanisms in Qiongzhusi Formation remain less understood compared to the Silurian Longmaxi Shale (Lu et al., 2019; Jiang et al., 2020). Previous research works on the Qiongzhusi Formation have proposed varying mechanisms, including the "productivity model" (Huang et al., 2019; Li et al., 2022) and "preservation model" (Wang et al., 2015; Babcock et al., 2015; Li et al., 2015), yet the role of orbital-scale processes in these mechanisms is not fully understood. Pan (2022) suggested that the primary productivity increased during the Maidiping Formation in the Sichuan Basin, and then decreased during the Qiongzhusi Formation with abundant growth of metazoa that dominating the entire marine ecosystem. Wang et al. (2007) proposed that increased primary productivity was a result of the combined effects of hydrothermal activity and upwelling currents, which is the main factors for organic matter accumulation. On the other hand, Li et al. (2022) argued that hydrothermal activity was the primary nutrients source and lead a high initial primary productivity during the Qiongzhusi Formation and it considered to be the main control factor of organic matter accumulation. Gu et al. (2022) pointed out that the primary productivity in lower part of Qiongzhusi Formation was at a relatively low level. Meanwhile, some researchers believed that organic matter accumulation was mainly influenced by redox condition variations (Zhou et al., 2020; Jin et al., 2014; Steiner et al., 2007). Zhou et al. (2020) demonstrated that the high productivity does not correspond to high total organic carbon content, the reason for this discrepancy may be the influence of suboxic marine water conditions.

This study acknowledges the significant impact of paleoenvironmental fluctuations and astronomical cycles on oceanic redox conditions, ecosystems, and biodiversity (Cronin and Raymo, 1997), which in turn affect the primary productivity of organic-rich shales. However, research specifically addressing the orbitally driven mechanisms of organic matter accumulation and its periodicity in the Qiongzhusi Formation of the Sichuan Basin remains sparse. Building on previous cyclostratigraphic studies (Liu et al., 2022; Zhou et al., 2022) and detailed sedimentological analyses (Zhang et al., 2022a), this study utilizes high-resolution TOC and Fe/Al series from Well JS103 for cyclostratigraphic analysis. Our scientific objectives are: (1) identify orbital parameters in TOC and Fe/Al series in Qiongzhusi Formation shales; (2) explore orbital forcing in organic matter accumulation in Lower Cambrian Qiongzhusi Formation shales; and (3) evaluate organic matter accumulation forcing mechanism based on the phase relationship of coupled series in terms of detrital input intensity and oceanic redox condition.

## 2. Geological background

### 2.1. Stratigraphy and tectonics

In the Early Cambrian period (~520 Ma), the South China Craton's Yangtze Block was an isolated craton positioned near the western coast of Gondwana at approximately 0° N (Merdith et al., 2017) (see Fig. 1A). The Sichuan Basin, covering and area of about 18 × $10^4$ $km^2$, was composed of six first-ordered tectonic units (Wei et al., 2014) (refer to Fig. 1B). The South China Block emerged from the collision of Cathaysia and Yangtze blocks in early Neoproterozoic Sibao-Jining Orogeny (Wang and Li, 2003) and its overall sedimentary thickness ranged from

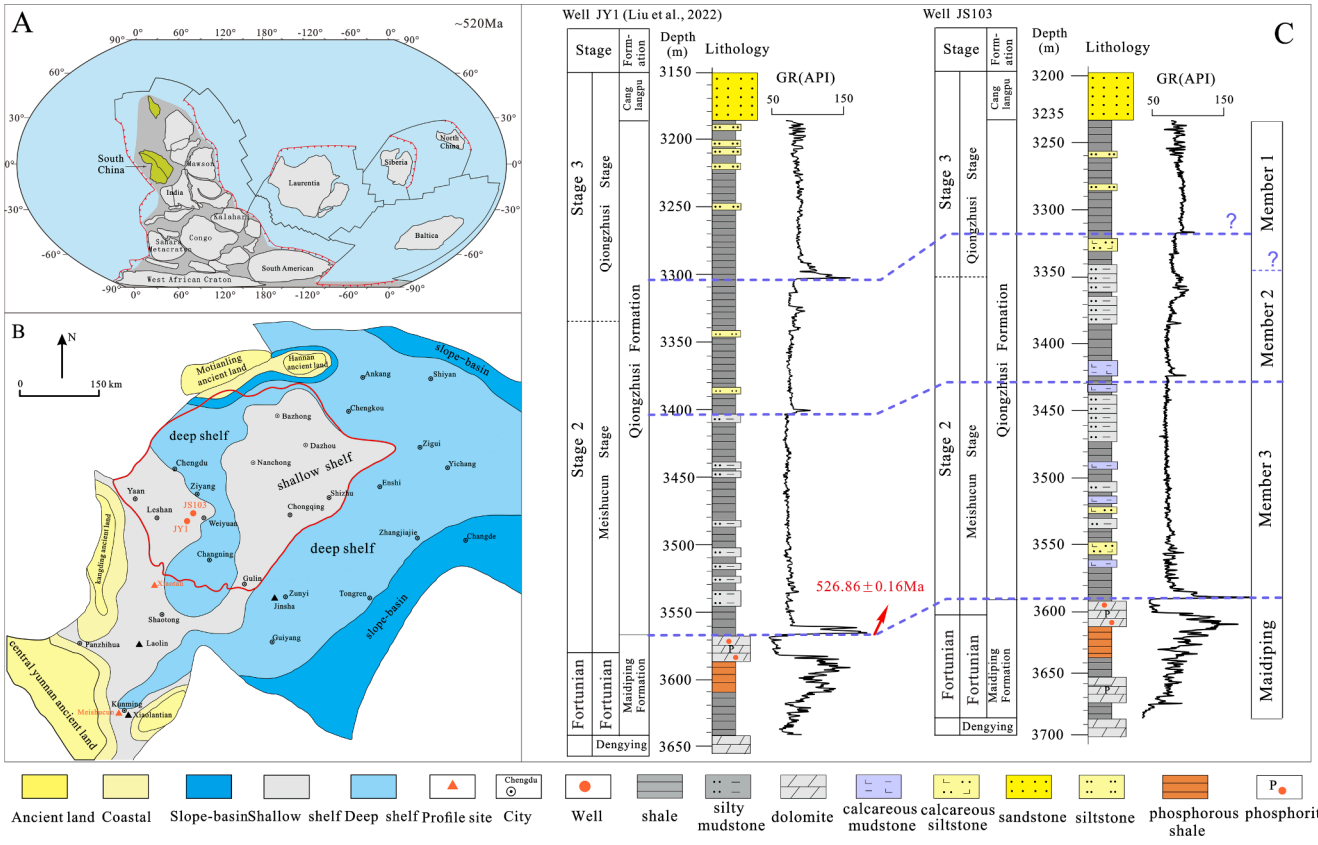


**Fig. 1.** (A) Global tectonic geography at 520 Ma (modified from Merdith et al., 2017) showing South China's location. (B) Paleogeography of South China (modified from Li et al., 2014) and location of Well JS103. (C) Comparison and correlation of stratigraphic framework between Well JY1 and JS103. Radiometric dates were obtained from Yang (2017) and Compston et al. (2008). The blue lines represent time equivalent horizons based on lithostratigraphy and biostratigraphy. The members' division of Well JY1 were cited from Liu et al. (2022), while the member division of Well JS103 was cited from Zhang et al. (2022b). (For interpretation of the references to color in this figure legend, the reader is referred to the web version of this article.)

$8 \times 10^3$ to $1.2 \times 10^4$ m. Vertically stratified, Dengying Formation is in a Sinian System and is predominantly composed of fine-grained silty dolomite, silty dolomite, micritic dolomite and argillaceous on the top (Fig. 2). The Tongwan movement created an unconformity between Dengying Formation and Cambrian System, resulting in an erosion depth of 50–200 m (Xu et al., 2012). The Cambrian system commenced with the Maidiping and Qiongzhusi Formations, mainly comprising shale with minor argillaceous siltstone components. These formations are notably the primary source rocks in central Sichuan Basin, especially in North Slope area and Ziyang-Changning rift trough (Fig. 1B).

### 2.2. Setting of Well JS103

The Southwest Oil and Gas Branch of Sinopec has recently undertaken a notable project in the Sichuan Basin, southwestern China, with the drilling of Well JS 103. This well is strategically located in the southwestern wing slope zone of the Weiyuan Structure. It has successfully tapped into the shale layers of the Qiongzhusi Formation. In a comprehensive drilling campaign, cores from the entire Qiongzhusi Formation (spanning depths from 3599.2 to 3304.5 m) were extracted, achieving an impressive near 100 % core recovery rate. The JS103HF exploration well has been particularly productive, yielding a high and stable flow of industrial gas. Its daily natural gas output has reached 258,600 cubic meters, leading to the identification and substantiation of significant geological resources estimated at 387.8 billion cubic meters.

Positioned in or adjacent to the intracratonic rift, specifically in the Ziyang-Changning area, Well JS103 intersects argillaceous shelf rocks. These rocks, with a substantial thickness ranging between 500 and 1000 m, are understood to have formed during the late Sinian to early Cambrian period, as per the findings of Liu et al. (2016). The lithostratigraphic analysis of Well JS103 reveals a 360-meter-thick sequence of the Qiongzhusi Formation, which is delineated into three distinct stratigraphic members, as illustrated in Fig. 1C. The composition of Members 2 and 3 is primarily characterized by black shale with pyrite nodules, grey calcareous mudstone, and silty shale. Conversely, Member 1 is predominantly composed of shale and argillaceous siltstone. This member is interspersed with fossil remnants such as *brachiopoda* and *trilobita*, along with biodetritus, highlighting its unique geological composition. In the adjacent region, Xiaotan section located in northeastern Yunnan (southwest of Yangtze Platform) provides a well-studied litho- and bio-stratigraphic records, offering valuable insights into stratigraphic correlations and depositional environments of the Early Cambrian (Och et al., 2013). Notably, the section reveals an erosional surface that demarcates the bulky grey dolomites of the Dengying Formation from siliceous micritic dolomites below. The Daibu Member in the Zhujiaqing Formation comprises chert and dolomite nodules on top, while the top of Yuanshan Formation features brownish siltstone with laminations and large cross-stratified sandstones of the Canglangpu Formation. The granular phosphatic dolomite and phosphatic rock assemblage in the intracratonic rifts (Ziyang-Changning area), such as the 30-meter-thick Maidiping Formation in Well JY1 (Changning area), correlate with the Zhujiaqing Formation in Xiaotan, Yunnan Province (Zhao et al., 2019; Och et al., 2013). Well JS103, in proximity to Well JY1, exhibits GR peaks at the Qiongzhusi and Maidiping Formation boundary, indicative of a highly radioactive uranium-enriched layer throughout the Sichuan Basin intracratonic rift (Gao et al., 2021; Liu et al., 2022) (Fig. 1C). Ash bed Zircons U-Pb ages from field outcrops like Xiaolantian, Laolin, and Meishucun sections in Yunnan Province have constrained the Early Cambrian time framework of in South China (e.g., Jenkins et al., 2002; Sawaki et al., 2008; Compston et al., 2008; Okada et al., 2014). A 526.5 ± 1.1 Ma U-Pb Zircon age was calibrated for the basal organic-rich Shiyantou Formation in the Meishucun section basal (Compston et al., 2008). Furthermore, Yang (2017) reportedd a new 526.86 ± 0.16 Ma CA-ID-TIMS zircon U-Pb age from the Meishucun sections, marking the boundary between the Qiongzhusi and Maidiping Formations. This study adopts the 526.86 ± 0.16 Ma age as the anchor point at Qiongzhusi Formation base, considering the continuous sedimentary successions in Well JS103during this period (Yang, 2017).

## 3. Data and methods

### 3.1. Well logs and geochemical proxies

In Well JS103, natural gamma spectral logging was used to quantify K, U, and Th contents. Elemental capture spectroscopy (ECS) logging measured the total organic carbon (TOC) series and high-resolution major element content series within the 3235–3585 m range of the Qiongzhusi Formation (Fig. 2). This study employed Fe/Al and TOC content series as proxies for cyclostratigraphy research. TOC data, widely recognized as a palaeoclimatic proxy, serves as a direct indicator of organic matter richness (Jin et al., 2020; Huang et al., 2021). The Fe content, normalized against Al (Fe/Al), is an effective measure of

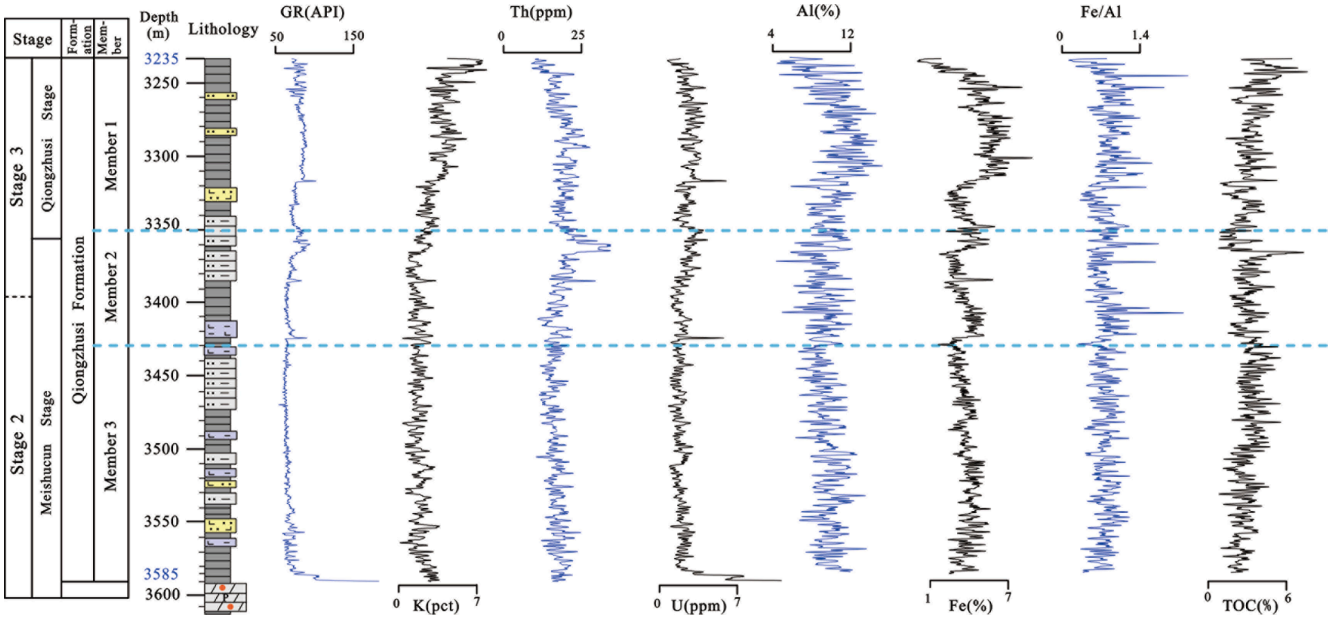


**Fig. 2.** The characteristic of well-logging curves (GR, K, Th, U, Al, Fe, Fe/Al, TOC) in Qiongzhusi Formation (3235–3585 m) of Well JS103.

siliciclastic sediment proportion, reflecting iron enrichment in sediments. Fluctuations in Fe/Al ratios are influenced by both benthic oxygen levels and detrital inputs. Geochemical data (Fe/Al and TOC) from Well JS103, collected at 0.1-m intervals, are included in supplementary material.

### 3.2. Correlation analysis

The analysis involved examining the correlation between two sets of logging data using a dynamic adjustable window in terms of depth and size. This technique produced a two-dimensional image, as illustrated in Fig. 3. In this image, depth was represented on the vertical axis, while the window size was depicted on the horizontal aixs. This graphical representation highlighted how the correlation between the logging datasets varied with changes in thickness and depth, as noted in the study by Peng et al. (2020a) and Liu et al.(2022). To conduct this correlation analysis, the "mwCor" function from "R" package "Astrochron" was utilized (Meyers and Sageman, 2007). The relevant scripts are available in supplementary section.

### 3.3. Time series analysis

#### 3.3.1. Preprocessing

Prior to identifying astronomical signals in paleoclimate proxy series, a crucial preparatory step involved linear interpolation in logging series to achieve evenly spaced data. A "Lowess smoother" technique, set to 15 %, was utilized to removed long-term trends. This step was essential to avoid and distortions in the low-frequency components of the spectra, as described by Li et al. (2019a). The *Acycle v 2.4.1* software was employed for preprocessing both the TOC and the raw Fe/Al series.

#### 3.3.2. Spectral estimation and filter

The Multitaper method (MTM, Thomson, 1982), combined with a robust red noise model, was instrumental in detecting astronomical signals within evolutionary fast Fourier transform (Evolutionary-FFT) spectrograms and detrended GR logging series. This approach is focused on the sequential exploration of frequency evolution, as detailed in the research by Kodama and Hinnov (2014). In this analysis, peaks that fell within 95 % and 99 % confidence intervals were specifically chosen for further examination.

The Evolutionary-FFT method not only presented the average power across the entire timespan of the series but was also pivotal in discerning variations in signal frequencies. This was achieved by employing a sliding window technique with varying widths. Such an approach enabled the calculation of different power levels at distinct cycle frequencies, which were identified from MTM spectra. This aspect of the analysis draws upon methodologies outlined in earlier studies by Kodama and Hinnov (2014) and Weedon (2003).

Additionally, the use of the Gaussian bandpass filter within the *Acycle v 2.4.1* software, a point noted in Li et al. (2019a), was particularly significant. This filter played a crucial role in isolating signals with a 405-thousand-year cycle, thereby allowing for a more focused analysis of these specific frequencies within the paleoclimatic data. This comprehensive approach, combining the MTM, Evolutionary-FFT, and Gaussian filtering, underlines a rigorous methodology in extracting and analyzing astronomical signals from paleoclimatic data series, ensuring a robust and reliable interpretation of the data.

#### 3.3.3. Correlation coefficient (COCO) analyses

The correlation coefficient (COCO) analyses (Li et al., 2018) assessed the most probable sedimentation rate, providing robust evidence for cyclostratigraphic interpretation. An enhanced version of this method, known as eCOCO, builds upon the original COCO framework. It effectively tracks changes in sedimentation rates by employing a windowed approach, allowing for a more dynamic and precise assessment. A key component of this methodology involved the use of Monte Carlo simulations. These simulations were crucial in evaluating the significance levels associated with the null hypothesis ($H_0$) that posits no astronomical forcing. This aspect of the analysis is elaborated upon in Li et al. (2019a), where the robustness of the eCOCO method in statistical testing is highlighted.

Furthermore, the determination of the maximum sedimentation rate was achieved by considering several factors. These included the maximum total number of astronomical parameters and the correlation coefficient, as well as the minimum value of the H0 hypothesis. This comprehensive approach, as detailed in the works of Li et al. (2018) and

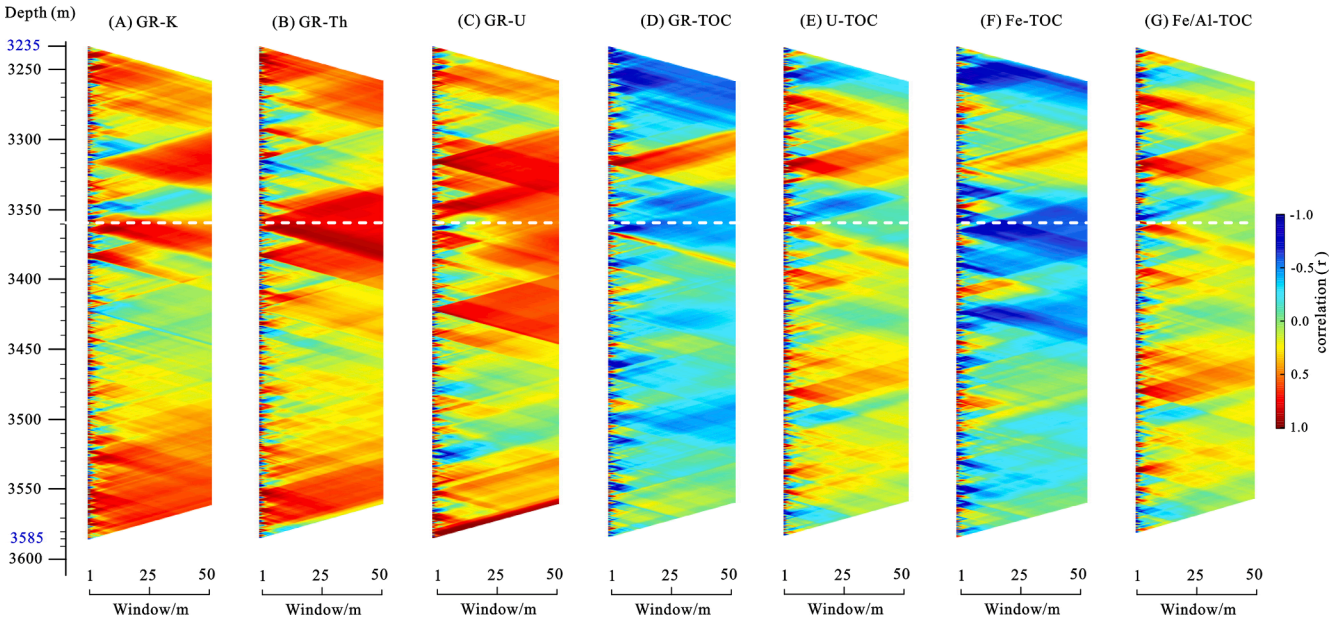


**Fig. 3.** The correlation analysis of (A) GR and K; (B) GR and Th; (C) GR and U; (D) GR and TOC; (E) U and TOC; (F) Fe and TOC; (G) Fe/Al ratio and TOC in Qiongzhusi Formation in Well JY1. The window was from 1 to 50 m. Red color indicates a positive correlation and blue color indicates a negative correlation. The scale indicates the window size (for the interpretation of references to color in this figure legend, the reader is referred to the web version of this article). (For interpretation of the references to color in this figure legend, the reader is referred to the web version of this article.)

Li et al. (2019a), underscores the method's ability to accurately identify and quantify sedimentation rates. The integration of these statistical tools and techniques enables a more nuanced understanding of sedimentary processes and their relationship with astronomical factors, thereby advancing the field of cyclostratigraphy.

### 3.4. Proxy spectra power decomposition analysis

The Power Decomposition Analysis (PDA) is a robust method used to estimate and compare the ratio of Milankovitchian power to the total power across various climate proxies, as detailed in the research by Li et al. (2019b). This ratio is crucial as it reflects the sensitivity of different proxies to climate forcing. In essence, the Milankovitchian-to-total power ratio serves as a measure of the signal-to-noise ratio within any given interval of the proxy data. Proxies that are more responsive to external climate variations typically exhibit higher values of this power ratio, indicating a stronger climate signal. This methodology was applied to the Gamma-Ray (GR) series, as highlighted in the study by Zhang et al. (2022b), as well as to the data series of iron/aluminum (Fe/Al) and total organic carbon (TOC). The PDA function in the *Acycle v 2.4.1* software was used for these analyses. This tool facilitated a detailed evaluation of the sensitivity of these proxies to external cyclic climate forces. As Li et al. (2019a) suggest, such an analysis is vital for understanding how different proxies record and respond to changes in Earth's climate system, particularly in the context of Milankovitch cycles.

The use of PDA in these studies exemplifies the advancement in methods to quantitatively assess proxy records. By accurately determining proxy sensitivity, researchers can better interpret past climate changes and refine models for future climate predictions. The PDA's ability to dissect and quantify the components of climate signals within proxy data represents a significant step forward in paleoclimatology and climatic cyclostratigraphy.

## 4. Results

### 4.1. Log response characteristics

Natural gamma-ray logs (GR, Th, U, K), along with Fe and Al logs, TOC series and Fe/Al ratio series from the Qiongzhusi Formation in Well JS103, are depicted in Fig. 2. Variations of K, GR, and Th logs were synchronous and closely tied to lithology, typically increasing with clay mineral content. However, U logs displayed a distinct pattern from K and Th, with several intervals in the Qiongzhusi Formation exhibiting high U values independent of lithology (Figs. 2 and 3). U enrichment, primarily formed through diagenesis in reducing conditions, resulted in these high values (Myers and Wignall, 1987). The correlation between various natural gamma spectrometry logging channels and GR logs is illustrated in Fig. 3. Higher GR emissions are often associated with clay-rich sediments, making GR logs useful for digitizing stratigraphy in the analysis of climatic cycles and paleoclimatic trends (De Vleeschouweret al., 2013). Also, Zhang et al. (2022b) adopted GR logs as proxy indicators of astronomically modulated climatic changes in Qiongzhusi Formation of Well JS103.

TOC, commonly used as a stratigraphic correlation and palaeoclimatic proxy tool due to its association with organic matter content (Rowe et al., 2008; Sageman et al., 2003; Liu et al., 2017). Jin et al. (2020), has also been employed in cyclostratigraphic studies by Jin et al. (2020). They found imprints of primary productivity or orbital forcing on bottom-water palaeoredox conditions in Early Silurian Longmaxi Formation shales in the Sichuan Basin. Cyclical TOC variations could be attributed to both detrital input and sea level fluctuation. Correlation of U logs with TOC series were observed, particularly in the 3300–3350 m depths of Member 1 of the Qiongzhusi Formation. The correlation of U logs with TOC series was even more pronounced than that for GR logs (Fig. 3).

Fe content, indicative of Fe enrichment in sediment, can be considered a marker of marine redox conditions. Normalized against Al (Fe/Al), it serves as a measure of siliciclastic sediment proportion (Raiswell and Canfield, 2012). Fe/Al series tracked terrestrial input variations influenced by astronomical forcing (Liu et al., 2021). Notably, the Fe/Al series showed similar trend to those in TOC series, suggesting a link between Fe content controlled by redox conditions and TOC content (Fig. 2).

### 4.2. Spectral analysis of Fe/Al and TOC series

The MTM power spectrum and evolutionary FFT spectrogram analyses of organic-rich shales within the Qiongzhusi Formation, specifically between the depths of 3235 and 3585 m, have uncovered noteworthy wavelengths in the Fe/Al and TOC series, as shown in Fig. 4A–D. These wavelengths demonstrated confidence levels exceeding 95 %, indicating a high degree of reliability in the findings. The observed sedimentary cycle ratios were found to be in close alignment with the Milankovitch periods predicted for the Cambrian era, as detailed in Waltham's, 2015 study. Specifically, wavelengths measuring approximately 14.9 and 20.7 m were linked to the 405-kyr eccentricity cycles. Additionally, the wavelength ranges of 9.7–4.7 and 4.4–3.1 m corresponded to the shorter ~100-kyr eccentricity cycles. Further analysis revealed that wavelengths between 2.1 and 1.4 and 2.6–1.5 m closely approximated the obliquity cycles. Despite the challenges posed by low sedimentation rates and the constraints of sampling resolution at the site, these sedimentary cycles provided critical insights. Notably, they indicated the absence of precession cycles, specifically the ~20 and ~16-kyr cycles referenced by Waltham (2015), in the Early Cambrian period in both the TOC and Fe/Al series from Well JS103.

As a result of these observations, the average sedimentation rates were calculated to be 3.67 cm/kyr and 5.11 cm/kyr for the respective data series. The COCO (Correlation Coefficient) analysis conducted subsequently lent further support to these findings.

### 4.3. Sedimentation rate of Well JS103

COCO analyses were performed on the Fe/Al and TOC series to determine the optimal sedimentation rate. Through 2000 Monte Carlo simulations, test sedimentation rates in Well JS103 ranged from 1 to 10 cm/kyr for both series (Fig. 5). Mean sedimentation rates for the Fe/Al series were above critical significance levels at 3.5 and 4.4 cm/kyr (Fig. 5A and D). eCOCO analyses indicated higher correlation coefficients for a sedimentation rate of 3.5 cm/kyr in the upper part (Member 1) of the Qiongzhusi Formation, with greater correlations at 4.4 cm/kyr in the lower part (Member 2 + 3). The sedimentation rate map of the Fe/Al series featured a shift around 3350 m (Fig. 5G), suggesting variations in sediment accumulation rate. Similarly, for the TOC series, mean rates of sedimentation at 1.8–2.5 and 7.6 cm/kyr exceeded the critical significance level (Fig. 5B and E). The mean sedimentation rate map (eCOCO) showed a pattern shift after 3350 m (Fig. 5H). Zhang et al. (2022) also revealed correlation coefficients among the power spectra of a time-calibrated GR series and astronomical solution by testing sedimentation rates in 1–10 cm/kyr range (Fig. 5C, F, and I). The COCO analysis of GR series identified several peaks at 2.2, 2.3, and 4.5 cm/kyr (Fig. 5C and F) and notable sedimentation rates were consistent with the 3.4–7.3 cm/kyr range reported by (Zhang et al., 2022b) for the three proxies (Fe/Al, TOC, and GR) across the entire Qiongzhusi Formation.

The sedimentation rate variation calculated by COCO/eCOCO analyses divided the studied interval (3235–3585 m) into two parts at the 3351 m boundary, corresponding to Members 1 and 2 of the Qiongzhusi Formation. The Fe/Al series of Member 1 of the Qiongzhusi Formation (3235–3351 m) exhibited significant sedimentary cycles with wavelengths indicative of 405-kyr long, ~100-kyr short eccentricity, and ~36-kyr obliquity cycles (Fig. 6E). Similarly, the Fe/Al series in

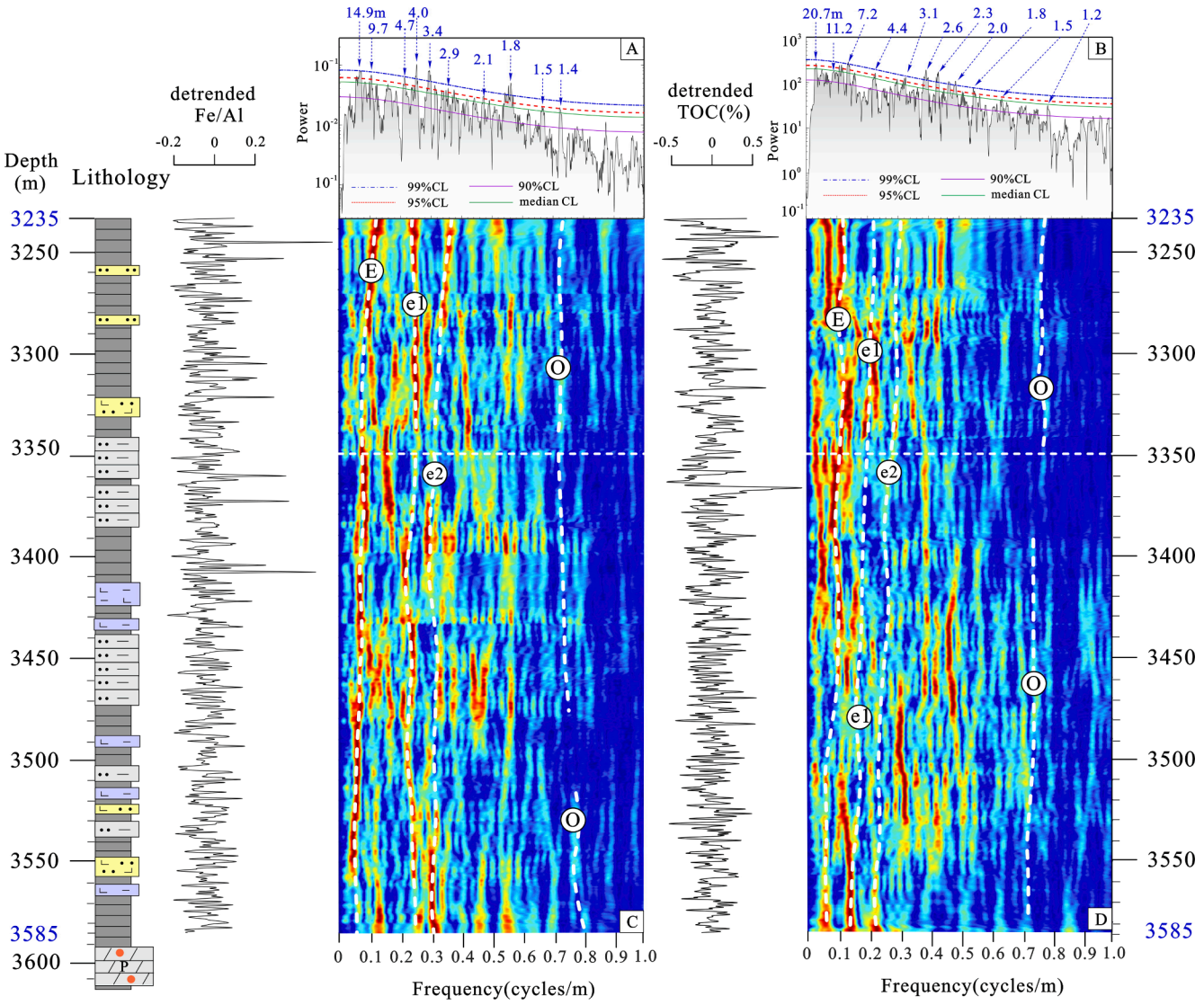


**Fig. 4.** 2π MTM spectra of (A) Fe/Al and (B) TOC series in Qiongzhusi Fm (3235–3585 m) of Well JS103. 2π MTM power spectrum is shown with median, 90 %, 95 %, and 99 % confidence levels. Fe/Al and TOC series were detrended by removing a 40-m LOWESS trend. The evolutionary power spectra of (C) Fe/Al and (D) TOC seires were calculated using a 50-m sliding window with a 0.5 m step. E = long eccentricity, e = short eccentricity, O = obliquity.

Members 2 and 3 (3351–3585 m) aligned with the same orbital cycles (Fig. 6F). The TOC series in Member 1 showed cycles corresponding to these orbital periods (Fig. 6G), and Members 2 and 3 displayed similar patterns (Fig. 6H). Gaussian bandpass filtering isolated ~11.2 m cycles in the Fe/Al series and ~10.80 m cycles in the TOC series of Member 1 (3235–3351 m), revealing 12 long eccentricity cycles (E1 to E12) (Fig. 6A and C). In Members 2 and 3 (3351–3585 m), ~15.6 m cycles in the Fe/Al series and ~16.7 m cycles in the TOC series were isolated, identifying 15 long eccentricity cycles (E13–E27) (Fig. 6B and D).

## 5. Discussion

### 5.1. *Cyclostratigraphy and the age anchor of Early Cambrian Qiongzhusi shale*

The geochemical periodicities observed in the Qiongzhusi shale's Fe/Al and TOC profiles are likely outcomes of various depositional and paleoclimate variances. These are predominantly linked to orbital cycles, as evidenced in recent studies (Jin et al., 2020; Zhao et al., 2023; Xiong et al., 2023). The congruence of Fe/Al and TOC series periodicities with dominant Early Cambrian obliquity, short and long eccentricity cycles, supports the theory of astronomical cycle pacing. The Floating astronomical time scale (FATS) for Early Cambrian Qiongzhusi shale at Well JS103 was calculated using the 405-kyr long eccentricity cycle, derived from both Fe/Al and TOC series. This cycle's stability and constancy, amplified by Jupiter's significant mass, make it an ideal Paleozoic time calibration marker (Laskar et al., 2004).

Using tuned Fe/Al and TOC series, we estimated early Cambrian shale durations in Qiongzhusi Formation in Well JS103 to be 10.790 and 10.792 Myr, respectively. Using a similar interval for the same borehole, Zhang et al. (2022b) employed a GR logging series from 3233 to 3591 m by tuning 405-kyr sedimentary cycles and calculated a ~10.80 Myr long high-resolution FATS. Furthermore, Liu et al. (2022) developed a FATS of ~10.87 Myr within Qiongzhusi Formation in Well JY1 located very close to Well JS103. Uncertainty in age model was due to the uncertainty of 0.2-Myr resulting from calculations using 405-kyr long eccentricity cycle.

The Early Cambrian time framework in South China is constrained by a series of radiometric ages that mainly obtained from the field outcrops from Meishucun, Laolin and Xiaolantian Sections in Yunnan Province (Jenkins et al., 2002; Sawaki et al., 2008). Three sets of widely distributed volcanic ash provided the zircons U-Pb ages that would

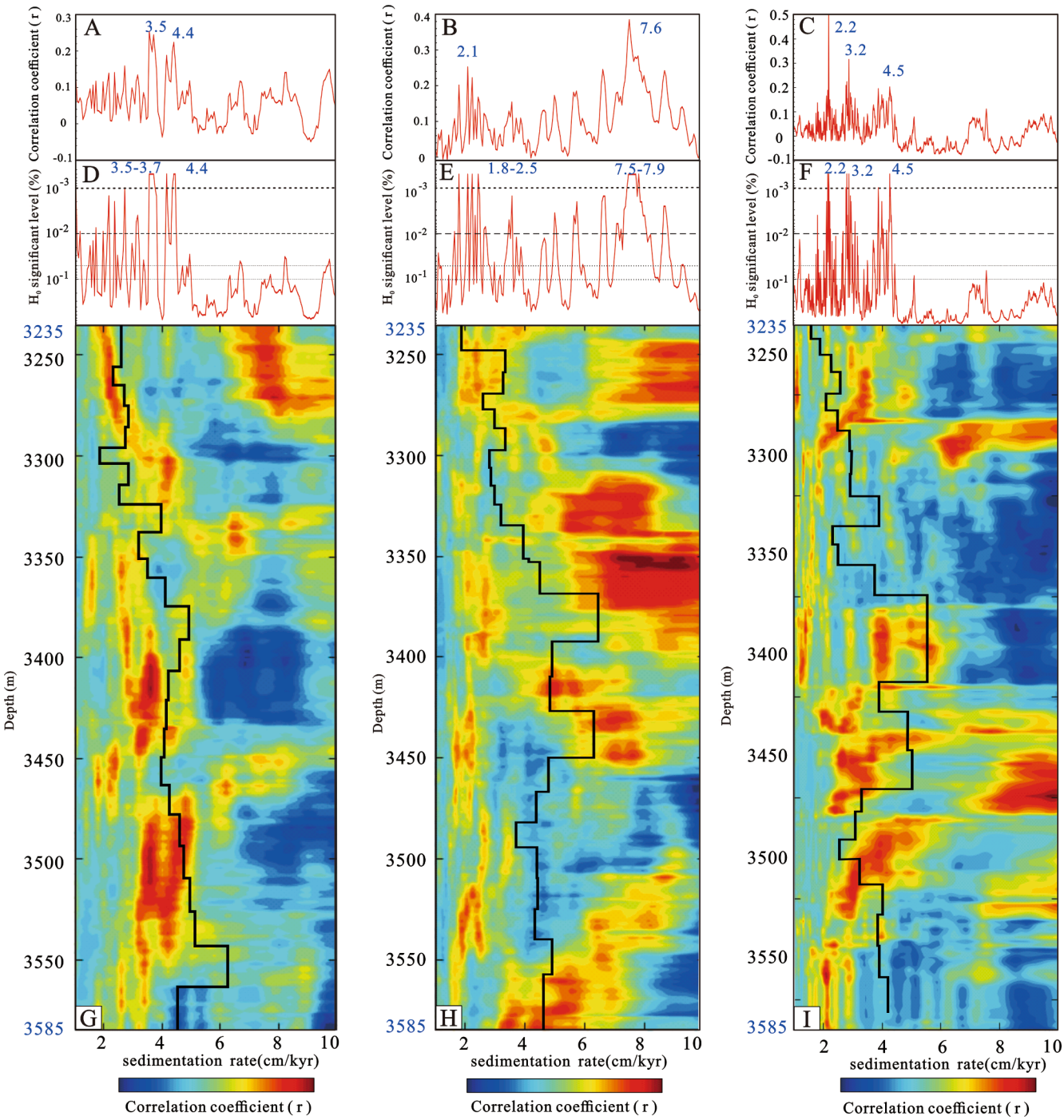


**Fig. 5.** The correlation coefficient and eCOCO analyses of untuned Fe/Al (A, D, G), TOC (B, E, H), and GR (C, F, I) series (Zhang et al., 2022b) in Qiongzhusi Formation (3235–3585 m). For both COCO and eCOCO analyses, testing sedimentation rates ranged from 1 to 10 cm/kyr with a step of 0.05 cm/kyr and the number of Monte Carlo simulations was 2000. eCOCO analysis was performed with a 50 m width sliding window. Black lines denote sedimentation rate curves based on long eccentricity tuning of statistically significant cycles in the three proxies from Wells JS103.

represent the depositional ages of the ash beds. A U-Pb Zircon age of 526.5 ± 1.1 Ma was determined for the basal organic-rich Shiyantou Formation at the Meishucun Section, Yunnan Province (Compston et al., 2008). The Meishucun Section is approximately 300 km from the Well JS103 location, indicating deposition of homogeneous black shale succession that started during the Cambrian Mid-Stage 2. Recently, Yang (2017) reported a new CA-ID-TIMS zircon U-Pb age of 526.86 ± 0.16 of the last appearance of SSFA-3 in Meishucun Section. In this study, the last appearance of SSFA-3 started with the base of black shale in Shiyantou Formation, and it can be regarded as the boundary at the bottom of Qiongzhusi Formation. Because Well JS103 developed a continuous sedimentary succession during the Qiongzhusi period, and the age of 526.86 ± 0.16 was adopted as the anchor point at the base of Qiongzhusi Formation. In this study, the Qiongzhusi Formation was calculated from 526.86 ± 0.16 to 516.06 ± 0.16 Ma of Well JS103, underwent a detailed cyclostratigraphic analysis. We employed the MTM (Multi-Taper Method) to transform the Fe/Al and TOC series from depth domain to time domain (Figs. 7A, 7B, 8B, and 8D). The transformation revealed distinct orbital cycle signals for eccentricity (~100 and 405-kyr) and obliquity (~36-kyr) in both series (Fig. 7C, 7D, 8B, and

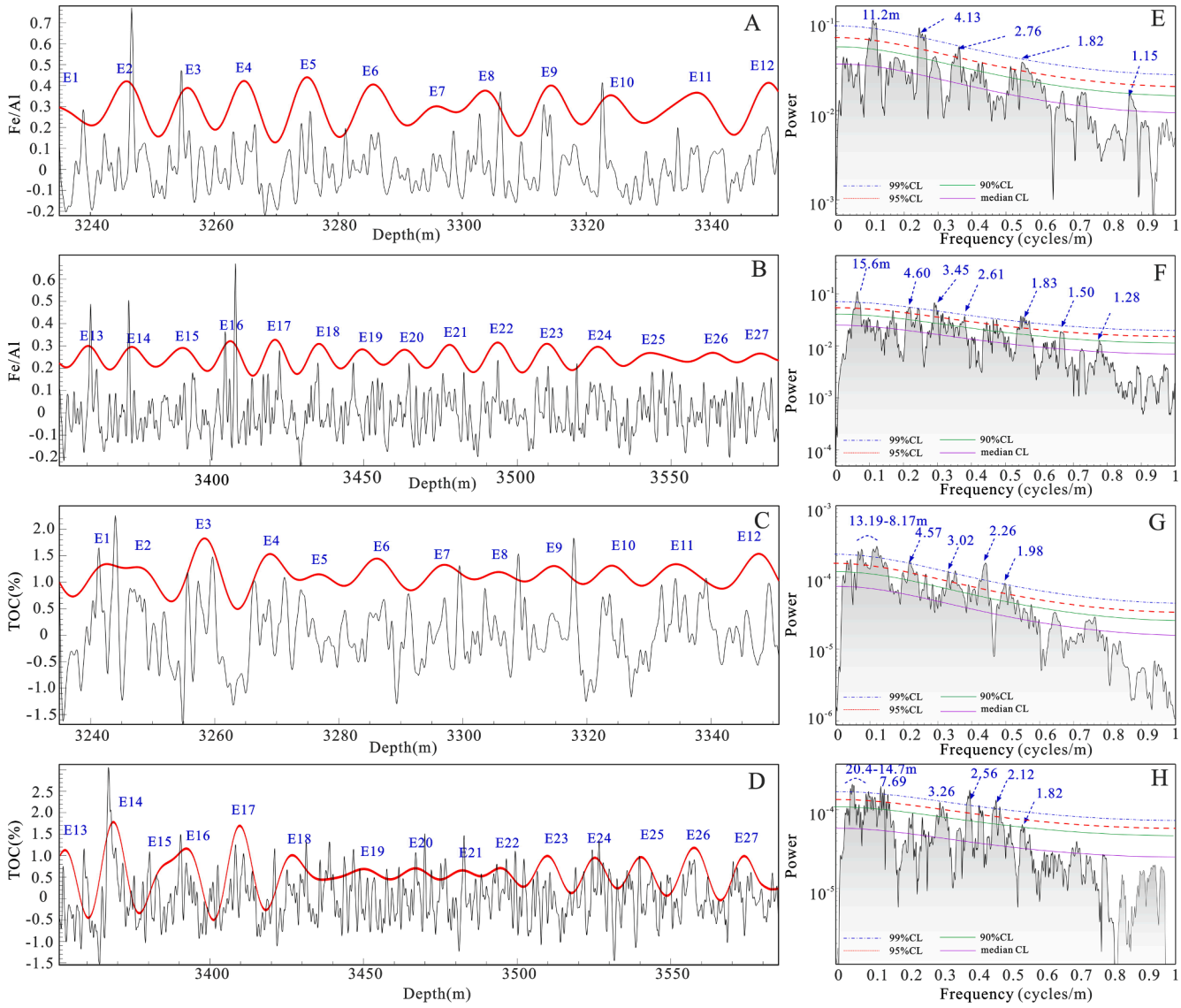


**Fig. 6.** Detrended Fe/Al and TOC series (left) of Qiongzhusi Formation. These are shown with interpreted long eccentricity cycles and their corresponding MTM power spectra with confidence levels (right). (A) Fe/Al series of Member 1 of Qiongzhusi Formation (3235–3351 m) with filtered ~11.20 m cycles (Gaussian filter with passband from 0.064 to 0.108 cycles/m). (B) Fe/Al series of Members 2 and 3 of Qiongzhusi Formation (3351–3585 m) with ~15.6 m cycles (Gaussian filter with passband from 0.054 to 0.08 cycles/m). (C) TOC series of Member 1 of Qiongzhusi Formation (3235–3351 m) with filtered ~10.8 m cycles (Gaussian filter with passband from 0.064 to 0.12 cycles/m). (D) TOC series of Middle and Lower Members (3351–3585 m) with ~16.7 m cycles (Gaussian filter with passband from 0.04 to 0.08 cycles/m). (E), (F), (G), and (H) illustrate 2π MTM spectra of Fe/Al and TOC series in (A), (B), (C) and (D), respectively.

8D). Notably, we observed significant long-tern amplitude modulation (AM) cycles in tuned TOC series (Fig. 9C). The presence of ~1.5-Myr obliquity AM cycles, identified independently and further supported by Zhang et al. (2022b) through dynamic noise after (DYNOT) orbital tuning analysis, suggests a link between long-term obliquity forcing and sea-level changes on a million-year scale (Fig. 9C and D).

To evaluate the relative responses of Fe/Al, TOC, and GR series to Milankovitch forcing, we applied the tuned proxy Power Decomposition Analysis (PDA) method. This involved adopting cutoff frequencies of 0.038–0.054, 0.022–0.030, and 0.001–0.015 $kyr^{-1}$ for precession, obliquity, and eccentricity, respectively. The oscillation in Fe/Al, GR and TOC series predominantly occurred within high signal-to-noise ratio Milankovitch bands (exceeding 80 %), as depicted in Fig. 8A, C, and E. Consequently, three proxies (Fe/Al, TOC, GR) demonstrated a high sensitivity to paleoclimate variations within Well JS103.

### *5.2. Eccentricity modulation of organic matter accumulation and shift phase relationship*

The Fe/Al and TOC series of Qiongzhusi shale records exhibit notable cycles within the long eccentricity band (405-kyr) (Figs. 7 and 9). A pronounced eccentricity signal in the TOC series, particularly highlighted in Fig. 8, suggests a modulation of organic matter accumulation by eccentricity in Qiongzhusi shales. Furthermore, the phase relationship between the Fe/Al and TOC series unveils new mechanisms of organic matter accumulation in the Early Cambrian Qiongzhusi Formation of the Sichuan Basin. These phase variations maybe linked to shifts in primary redox and productivity conditions relevant organic matter accumulation (Huang et al., 2022).

The Fe/Al series reflects two factors: redox conditions (indicated by Fe content) and terrestrial sediment influx (represented by Al content). Variations in Fe/Al ratio are primarily influenced by benthic oxygen levels and detrital inputs, both of which are likely affected by the intensity of orbital-scale monsoon. These monsoons impact detrital input,

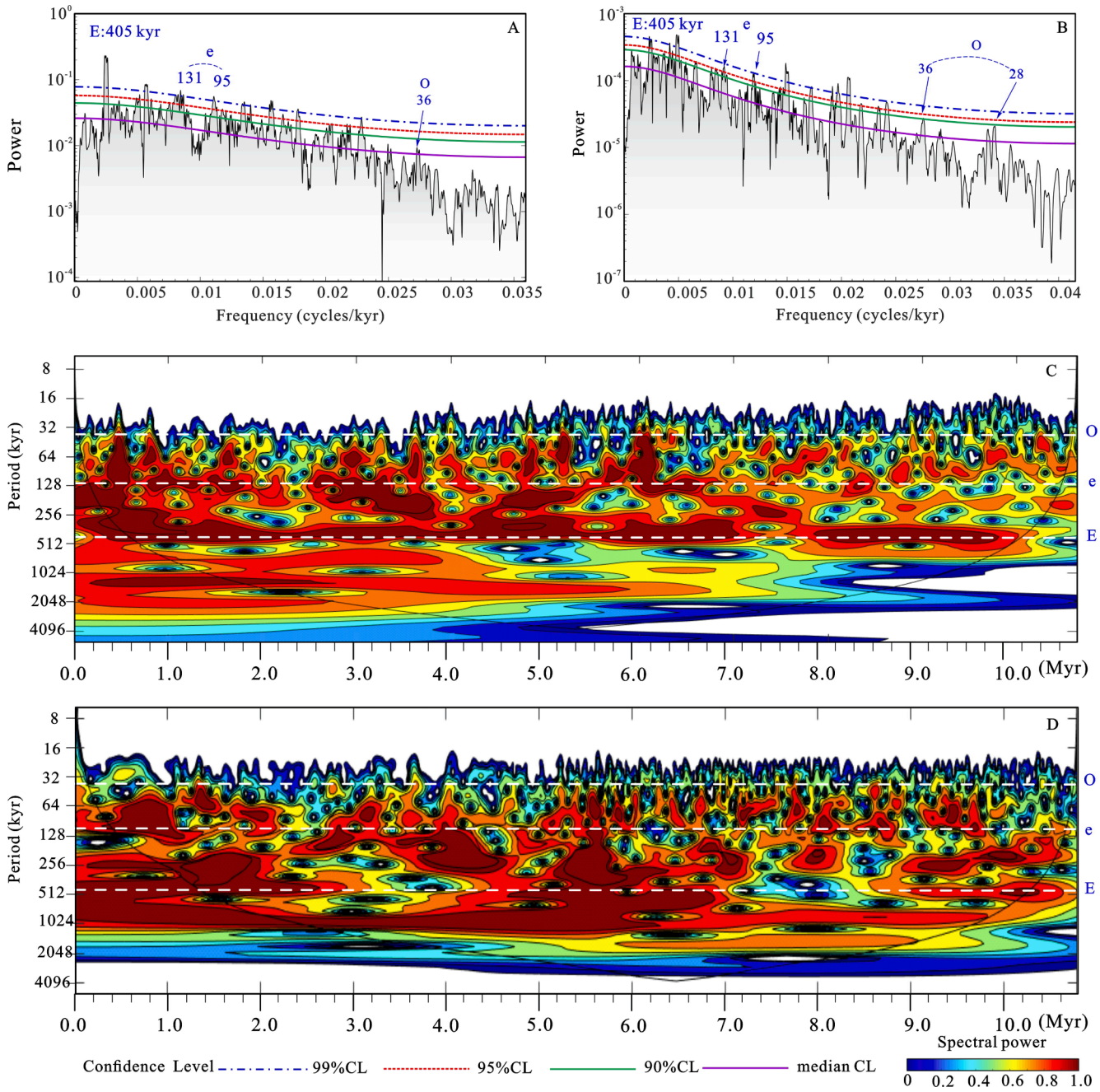


**Fig. 7.** Results of cyclostratigraphic analysis in time domain. (A) The 2π MTM spectrum of the 405-kyr tuned Fe/Al series of Well JS103. (B) The 2π MTM spectrum of the 405-kyr tuned TOC series of Well JS103. (C) The wavelet transform (WT) scalogram of 405-kyr tuned Fe/Al series at Well JS103. (D) The wavelet transform (WT) scalogram of 405-kyr tuned TOC series at Well JS103. Frequency peaks of astronomical cycles are illustrated with white dashed lines.

terrigenous nutrient levels, and regional upwelling (Berger et al., 1989; Yan et al., 2015). High Fe/Al values correlating with elevated TOC levels imply stable anoxic conditions conducive to organic matter accumulation, coupled with reduced nutrient flux due to weaker monsoonal rainfalls. Conversely, monsoon-driven productivity variations tied to orbital cycles could create antiphase relationships between Fe/Al and TOC. Enhanced monsoon circulation, by boosting nutrient supply through increased upwelling and river runoff, might trigger productivity blooms, thus augmenting organic matter accumulation. Therefore, instances of low Fe/Al values in antiphase with high TOC levels could be attributed to increased productivity from intensified monsoon activity driven by orbital dynamics. This sensitivity to monsoon variations, especially in the context of Early Cambrian climate, aligns with the documented influence of Intertropical Convergence Zone dynamics and low latitude climate processes (Zhang et al., 2022b), further corroborated by the prevalence of eccentricity cycles in Cambrian strata (Zhang et al., 2022b; Sørensen et al., 2020; Fang et al., 2020).

During in-phase intervals, concurrent increases in Fe/Al and TOC values at times of eccentricity minimum are hypothesized to reflect reduced weathering under weakened monsoonal conditions driven by precessional forcing in low-latitude climates. This pattern, indicative of a "preservation-mode" of organic matter accumulation, is evident in Fig. 10B. In contrast, the observed anti-phase relationship between Fe/Al and TOC, with decreased Fe/Al potentially recording heightened nutrient supply due to increased weathering and amplified monsoon intensification, suggests a "productivity-mode" of organic matter accumulation, as illustrated in Fig. 10A.

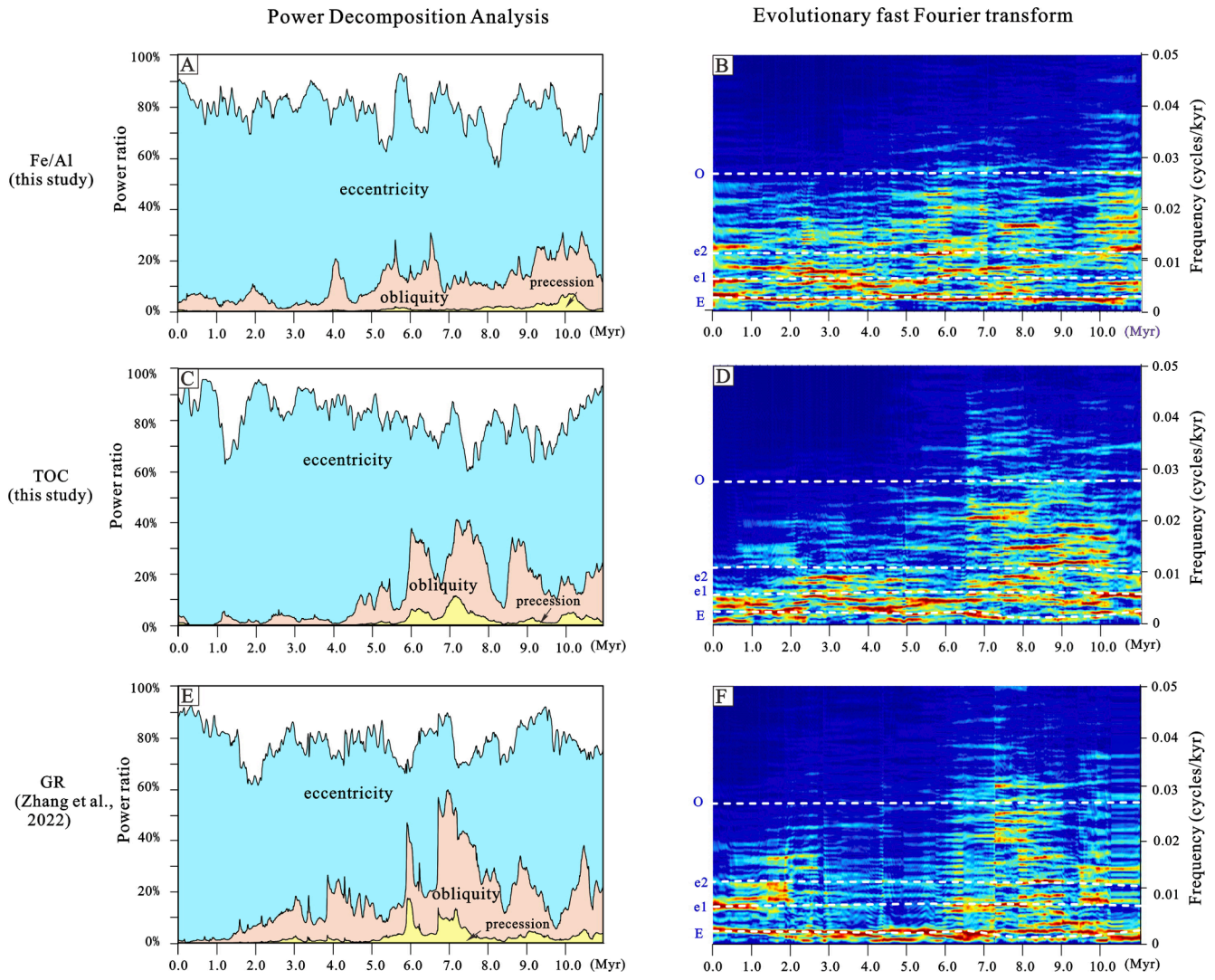


**Fig. 8.** Power decomposition analysis (left) and evolutive FFT spectra (right) of tuned Fe/Al ratio, TOC and GR series in Well JS103 of Qiongzhusi Formation in Sichuan Basin. (A) Power decomposition analysis (PDA) of Fe/Al ratio series; (B) evolutive FFT spectra of Fe/Al ratio series; (C) PDA of TOC series; (D) evolutive FFT spectra of TOC o series; (E) PDA of GR series (GR data are cited from Zhang et al., 2022b); (F) evolutive FFT spectra of GR series (Zhang et al., 2022b). Passbands of eccentricity, obliquity and precession for PDA are 0.001–0.015, 0.022–0.04, and 0.038–0.054 $kyr^{-1}$, respectively.

### *5.3. ~1.5-Myr timescale orbital variation of organic matter accumulation*

The analysis of the Early Cambrian Qiongzhusi Formation provides novel insights into the interplay between short-term (405-kyr) and long-term (~1.5-Myr) orbital variations and their influence on organic matter accumulation. Zhang et al. (2022a) identified ~1.5-Myr cycles in the DYNOT median curve, suggesting a linkage between long-term ($s_4$-$s_3$) cycle forcing and sea-level change on a million-year scale (Fig. 9D, purple curves). Our study corroborates this by observing similar ~1.5-Myr cycles in the obliquity amplitude modulation curves within the Fe/Al series (Fig. 9C, purple curves).

Sea-level rise can generally be attributed to two primary factors: tectonic and climatic changes (Hamlington et al., 2021). While tectonic forces appear to exert minimal influence on the TOC variations of this organic-rich shale, climatic changes impacting redox conditions and productivity likely cause phase shifts between TOC and redox-sensitive elements. The observed phase shifts in our study align with the DYNOT model predictions driven by sea-level fluctuations. The modulation of Earth-Sun distance affects solar radiation received on Earth. Increased obliquity enhances insolation in high-altitude areas and decreases it during winter; intensifying seasonal variations (Liu et al., 2019; Cao et al., 2022). We observed a transfer of obliquity amplitude modulation signals from high-latitude regions to the equatorial areas in Well JS103. The ~1.5-Myr cycles in the TOC series, alongside the ~1.5-Myr DYNOT cycles, depict a shift from in-phase to anti-phase relationships within the Qiongzhusi Formation (Fig. 9C, D).

Rising sea levels, particularly in deep oceanic basins, tend to create more restricted and oxygen-depleted environments. This scenario likely enhanced the organic matter preservation, with the sea-level variations aligning with TOC changes at the ~1.5-Myr cycles. During in-phase intervals, increased sea level is speculated to boost organic matter accumulation under stable anoxic conditions. Conversely, anti-phase periods between the ~1.5-Myr-filtered TOC series and the ~1.5-Myr-filtered DYNOT curves indicate enhanced moisture and heat flux, leading to sea level rise. This corresponds to increased atmospheric-ocean thermal gradients, de-stratification of water column, and improved oxygenation, resulting in less effective of organic matter preservation (Fig. 9C, D). These obliquity amplitude modulation signals in the Qiongzhusi Formation provide a record of varying geographic sensitivities to orbital forcing, influencing both organic matter accumulation and broader climate dynamics.

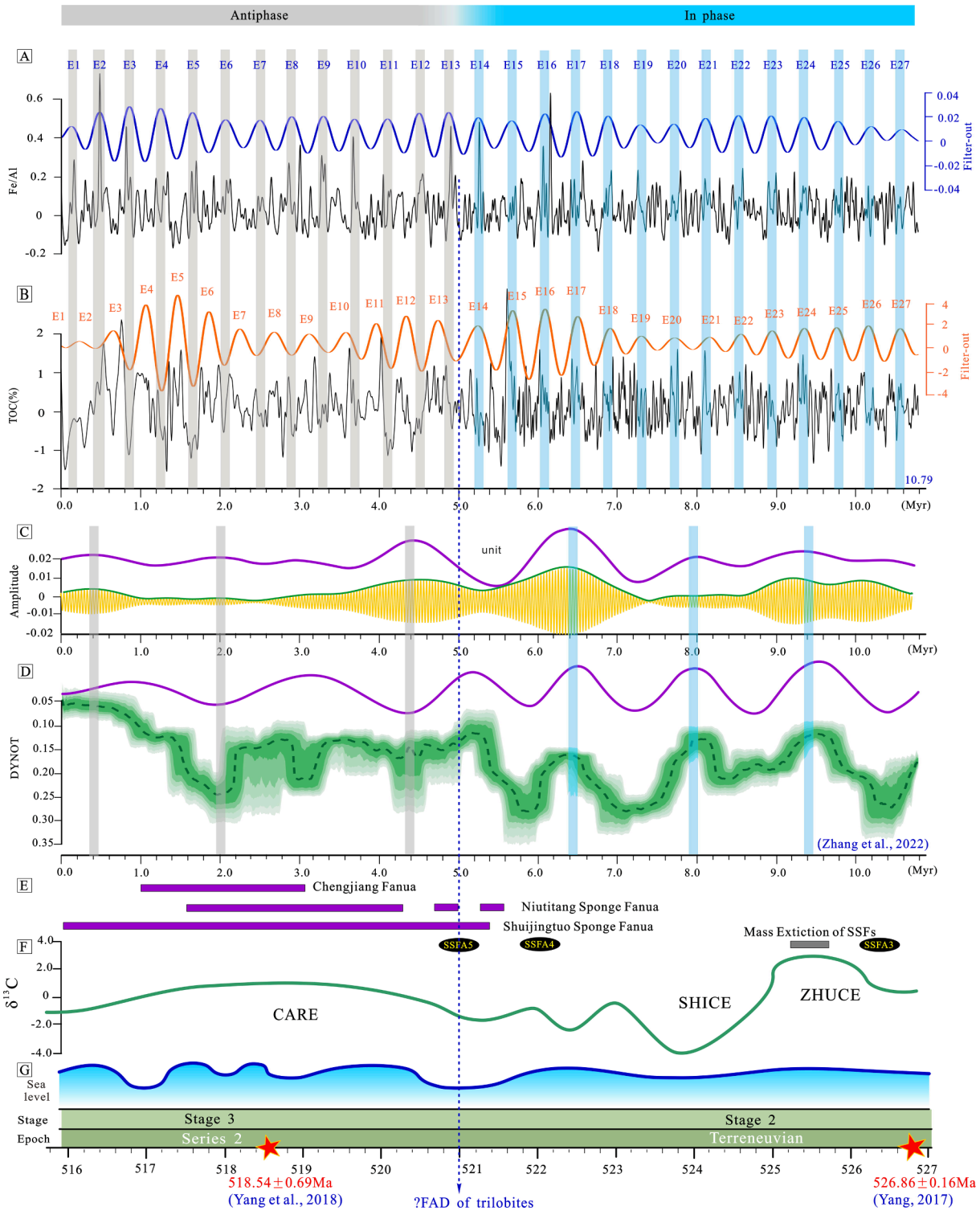


**Fig. 9.** Phase relationship of stratigraphic changes between tuned Fe/Al ratio and TOC series on 405-kyr cycles at Well JS103. (A) Tuned Fe/Al series (black lines) with 405-kyr-filtered output (purple lines). (B) Tuned TOC series (black lines) with 405-kyr-filtered output (orange lines). (C) Amplitude modification of obliquity signal in 405-kyr tuned TOC series (Gaussian passband from 0.0004 to 0.0008 cycles/kyr). (D) DYNOT results of 405-kyr tuned GR series were taken from Zhang et al. (2022b) and ~1.5-Myr cycles filter output (passband from 0.0004 to 0.0008 cycles/kyr) (Zhang et al., 2022b) (E) Major biological event during "Cambrian explosion" (Peng et al., 2020b); the appearance of small shelly fossils assemblages 3–5 is taken from Jin et al. (2016) and Steiner et al. (2007). (F) The $\delta^{13}C_{carb}$ curve was modified from Zhu et al. (2006). (G) Global sea-level curve during the early Cambrian (after Snedden and Liu, 2010). (For interpretation of the references to color in this figure legend, the reader is referred to the web version of this article.)

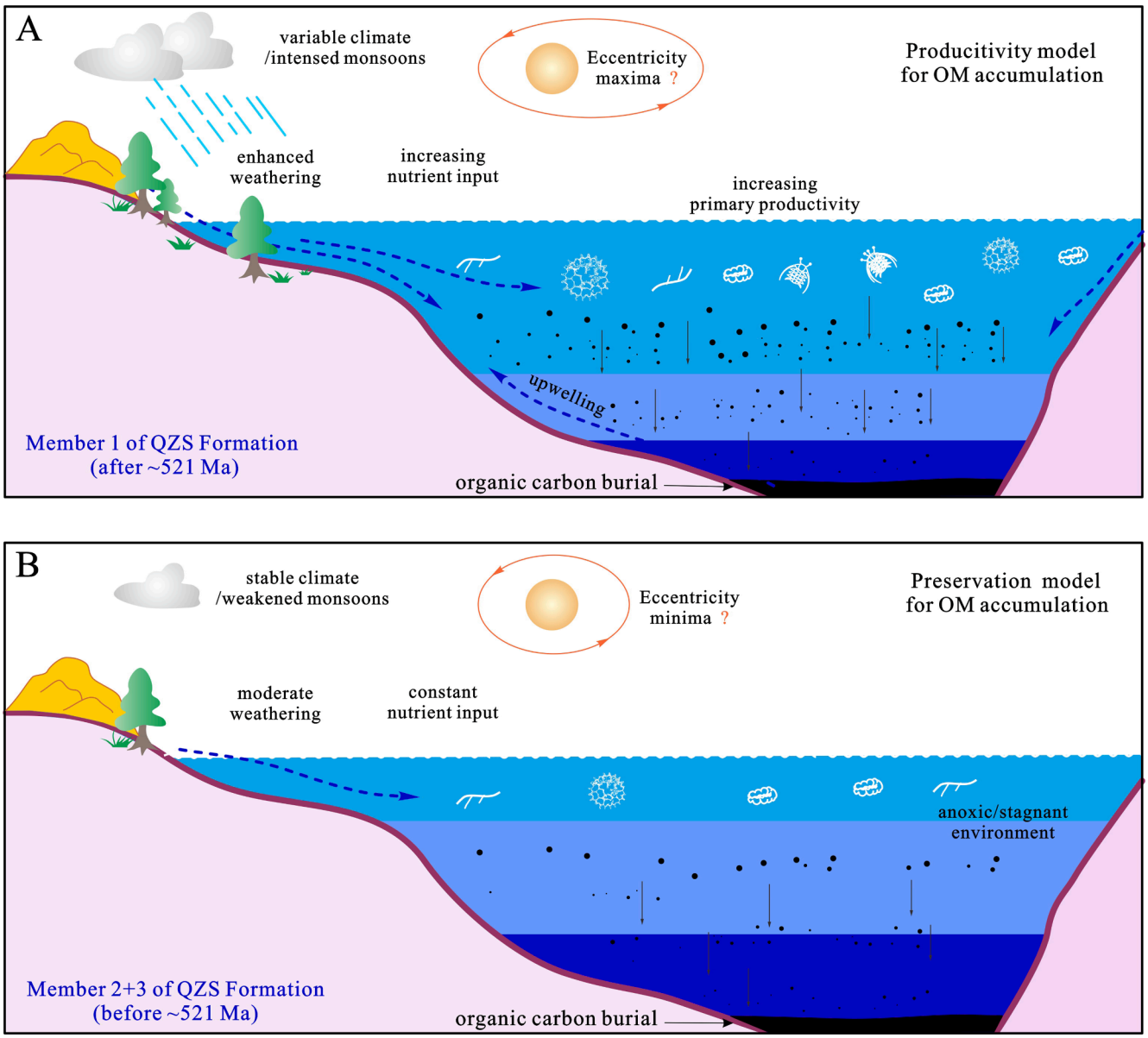


**Fig. 10.** Two models for organic matter accumulation in Qiongzhusi Formation, Sichuan Basin. (A) High productivity model with intensified monsoon and nutrient supply in Member 1 of Qiongzhusi Formation (after ~521 Ma). (B) Preservation model with weakened monsoons and prolonged organic matter burial in Member 2 and 3 of Qiongzhusi Formation (before ~521 Ma).

### *5.4. The trigger of "second Cambrian explosion": Orbitally driven?*

Cyclostratigraphic analysis, especially the examination of phase relationships among various proxy series, serves as a pivotal tool for deciphering the orbital-driven sedimentation processes and climate variation. Prior research has demonstrated that analyzing multiple proxies can elucidate the interplay between orbital parameters and paleoenvironment changes (Ikeda et al., 2016; Li et al., 2017). Li et al. (2017) claimed that shifts in phasing marks a wholesale dramatic oceanographic change, marking the end of OAE2. Similarly, Ikeda et al. (2016) noted that shifts in the abundance and color of chert correlated with glacio-eustatic sea-level changes akin to those during the Oligocene to Pliocene glacial cycles. Wehausen and Brumsack (2002) explained that the antiphase relationship of Ba/Al and K/Si ratios suggested opposing patterns in summer and winter monsoons, particularly in Pliocene South China Sea.

In this study, the synchronous phase shift observed in the 405-kyr-filtered curves of TOC and Fe/Al series (Fig. 9A, B), as well as the ~1.5-Myr-filtered curves of TOC and DYNOT (Fig. 9C, D), implies a link between intensified climate changes and disruptions in oceanic oxygen levels, potentially affecting biological recovery. It's important to highlight that the observed phase shift took place at the junction between the upper (Member 1) and lower (Member 2) sections of the Qiongzhusi Formation. This juncture could potentially result in signal discontinuity and phase shifts. Throughout the data analysis and processing, particularly in the sliding window spectrum analysis and the eCOCO analysis, the signal discontinuities of the three proxies (Fe/Al, TOC and GR) were evident in the imagery of the whole section (Figs. 4 and 5). This observation suggests that the changes in the signal were not merely a result of segmentation in the processing but were more likely attributable to significant geological events or environmental shifts occurring at these depths.

This phase shift, occurring around ~521 Ma. (Fig. 9), coincides with the emergence of Niutitang and Shuijingtuo Spange Fanuas (Fig. 9E), suggesting that Cambrian biodiversification might have been spurred by increased primary productivity driven by astronomical forcing after

~521 Ma. The stepwise oxygenation of ocean surface layers, paralleled by a gradual increase in ecosystem complexity in lower Cambrian strata (Jin et al., 2016), points to a potential orbital influence on the "Second Cambrian Explosion" in South China. Furthermore, the mass extinction of small shelly fossils (SSFs) during the Early Cambrian appears to correspond with a sea-level rise driven by ~1.5-Myr-filtered obliquity amplitude modulation signals. This relationship suggests that the expansion of anoxic bottom water played a significant role in the SSFs mass extinction.

Therefore, these interconnections between orbital-driven sea-level variations, organic matter accumulation, and the patterns of biological extinction and recovery during the Early Cambrian Qiongzhusi Formation offer valuable insights into the mechanisms of carbon cycling and climate dynamics during this critical geological period.

## 6. Conclusions

This study has successfully established an approximately 10.8 Myr long astronomical time scale for the Lower Cambrian Qiongzhusi Shales in Well JS103. This was achieved by astronomically tuning the Fe/Al and TOC series to the stable 405-kyr cycles. The stratigraphic variations observed in the Fe/Al series presented cycles of about 11.20 and 15.6 m, while the TOC series depicted cycles of approximately 10.8 and 16.7 m. These cycles correspond to the 405-kyr long eccentricity cycles and agree with both the COCO analysis and previous cyclostratigraphic analyses.

The phase relationships within the 405-kyr and ~1.5-Myr orbital cycles revealed a transition from antiphase to in-phase relationships around ~521 Ma. This period marks a significant shift in the Cambrian bio-radiation, driven by an increase in atmospheric and oceanic oxygen level post ~521 Ma. Prior to this, marine conditions were characterized by restricted, anoxic bottom waters, which likely hindered ecosystem recovery and could have been influenced by astronomical forcing. The cyclostratigraphic analyses conducted in this study provide a new insight into the processes of organic matter accumulation, particularly in relation to oceanic redox dynamics and biological innovations during the Early Cambrian periods.

## CRediT authorship contribution statement

**Siding Jin:** Writing – review & editing, Writing – original draft, Funding acquisition, Data curation, Conceptualization. **Yan Liu:** Writing – original draft, Validation, Resources, Project administration, Conceptualization. **Chao Ma:** Visualization, Supervision, Methodology, Funding acquisition, Formal analysis. **Quanlin Zhang:** Validation, Resources. **Anqing Chen:** Supervision, Funding acquisition.

## Declaration of competing interest

The authors declare that they have no known competing financial interests or personal relationships that could have appeared to influence the work reported in this paper.

## Data availability

Data will be made available on request.

## Acknowledgements

We gratefully acknowledge the support provided by the National Natural Science Foundation of China, with specific thanks to the grants No. 41802030, No. 41888101, No. 42172137 and No. 42272132. Additional support was received from the Sichuan Provincial Youth Science & Technology Innovative Research Group Fund (No. 2022JDTD0004). This work is a contribution to the Deep-time Digital Earth (DDE) Big Science Programs and IGCP 739. We extend our sincere appreciation to all reviewers who participated in the review process, whose insights and critiques have been invaluable to this study.

## Appendix A. Supplementary material

Supplementary data to this article can be found online at https://doi.org/10.1016/j.jseaes.2024.106033.

## References

Babcock, L., Peng, S.C., Brett, C., Zhu, M.Y., Ahlberg, P., Bevis, M., Robison, R.A., 2015. Global climate, sea level cycles, and biotic events in the Cambrian period. Palaeoworld 24 (1–2), 5–15.

Berger, W.H., Smetacek, V.S., Wefer, G., 1989. Ocean productivity and paleoproductivity an overview. In: Berger, W.H., Smetacek, V.S., Wefer, G. (Eds.), Productivity of the Ocean: Present and past. Wiley, Chichester, pp. 1–34.

Berner, R.A., 1990. Atmospheric carbon dioxide levels over phanerozoic time. Science 249 (4975), 1382–1386.

Bjørlykke, K.O., 2010. Petroleum Geoscience: From Sedimentary Environments to Rock Physics. Springer-Verlag, Berlin.

Bosmans, J.H.C., van der Ent, R.J., Haarmsa, R.J., Drijfhout, S.S., Hilgen, F.J., 2020. Precession- and obliquity- induced changes in moisture sources for enhanced precipitation over the Mediterranean Sea. Paleoceanogr. Paleoclimatol. 35, e2019PA003655.

Canuel, E.A., Cammer, S.S., McIntosh, H.A., Pondell, C.R., 2012. Climate change impacts on the organic carbon cycle at the land-ocean interface. Annu. Rev. Earth Planet. Sci. 40, 685–711.

Cao, H.Y., Jin, S.D., Hou, M.C., Chen, S., Liu, Y., Chen, A.Q., 2022. Astronomical cycles calibrated the sea-level sequence durations of Late Miocene to Pliocene in Qiongdongnan Basin, south China Sea. Mar. Pet. Geol. 143, 105813.

Charbonnier, G., Boulila, S., Spangenberg, J.E., Adatte, T., Föllmi, K.B., Laskar, J., 2018. Obliquity pacing of the hydrological cycle during the Oceanic Anoxic Event 2. Earth Planet. Sci. Lett. 499, 266–277.

Compston, W., Zhang, Z., Cooper, J.A., Ma, G.G., Jenkins, R.J.F., 2008. Further SHRIMP geochronology on the early Cambrian of South China. Am. J. Sci. 308, 399–420.

Cronin, T.M., Raymo, M.E., 1997. Orbital forcing of deep-sea benthic species diversity. Nature 385, 624–627.

De Vleeschouwer, D., Rakociński, M., Racki, G., Bond, D.P.G., Sobień, K., Claeys, P., 2013. The astronomical rhythm of Late-Devonian climate change (Kowala section, Holy Cross Mountains, Poland). Earth Planet. Sci. Lett. 365, 25–37.

Eldrett, J.S., Ma, C., Bergman, S.C., Ozkan, A., Minisini, D., Lutz, B., Jackett, S.J., Macaulay, C., Kelly, A.E., 2015. Origin of limestone–marlstone cycles: Astronomic forcing of organic-rich sedimentary rocks from the Cenomanian to early Coniacian of the Cretaceous Western Interior Seaway, USA. Earth Planet. Sci. Lett. 423, 98–113.

Fang, J.C., Wu, H.C., Fang, Q., Shi, M.N., Zhang, S.H., Yang, T.S., Li, H.Y., Cao, L.W., 2020. Cyclostratigraphy of the global stratotype section and point (GSSP) of the basal Guzhangian Stage of the Cambrain Period. Paleogeogr. Paleoclimatol. Paleoecol. 540, 109530.

Gao, P., Li, S.J., Lash, G.G., Yan, D.T., Zhou, Q., Xiao, X.M., 2021. Stratigraphic framework, redox history, and organic matter accumulation of an Early Cambrian intraplatform basin on the Yangtze Platform, South China. Mar. Pet. Geol. 130, 105095.

Gu, H., Wang, J., Wei, H.Y., Fu, X.G., 2022. Controlling factors of organic enrichment in the Shuijingtuo Formation in the Lower Cambrian of the Chengkou Area, Sichuan Basin. Acta Seimentol. Sin. doi: 10.14027/j.issn.1000-0550.2022.091.

Hamlington, B.D., Frederikse, T., Thompson, P.R., Willis, J.K., Nerem, R.S., Fasullo, J.T., 2021. Past, present, and future Pacific Sea-level change. Earth's Future 9 (4), e2020EF001839.

Herrle, J.O., Pross, J., Friedrich, O., Köβler, P., Hemleben, C., 2003. Forcing mechanisms for mid-Cretaceous black shale formation: evidence from the Upper Aptian and Lower Albian of the Vocontian Basin (SE France). Palaeogeogr. Palaeoclimatol. Palaeoecol. 190, 399–426.

Hesselbo, S.P., Morgans-Bell, H.S., McElwain, J.C., Rees, P.M., Robinson, S.A., Ross, C.E., 2003. Carbon-cycle perturbation in the middle Jurassic and accompanying changes in the terrestrial paleoenvironment. J. Geol. 111 (3), 259–276.

Huang, T.Y., Chen, D.Z., Fu, Y., Yeasmin, R., Guo, C., 2019. Development and evolution of a euxinic wedge on the ferruginous outer shelf of the early Cambrian Yangtze Sea. Chem. Geol. 524, 25–271.

Huang, H., Gao, Y., Ma, C., Jones, M.M., Zeeden, C., Ibarra, D.E., Wu, H., Wang, C., 2021. Organic carbon burial is paced by a ~173-ka obliquity cycle in the middle to high latitudes. Sci. Adv. 7, eabf9489.

Huang, W., Wu, H., Fang, Q., Zhang, S., Yang, T., Li, H., Shi, M., 2022. Orbitally forced organic matter accumulation recorded in an Early Permian mid-latitude palaeolake. Palaeogeogr. Palaeoclimatol. Palaeoecol. 606, 111259.

Ikeda, M., Bôle, M., Baumgartner, P.O., 2016. Orbital-scale changes in redox condition and biogenic silica/detrital fluxes of the Middle Jurassic Radiolarite in Tethys (Sogno, Lombardy, N-Italy): possible link with glaciation? Paleogeogr. Paleoclimatol. Paleoecol. 457, 247–257.

Jenkins, R.J.E., Cooper, J.A., Compston, W., 2002. Age and biostratigraphy of Early Cambrian tuffs from SE Australia and southern China. J. Geol. Soc. Lond. 159 (6), 645–658.

Jiang, Z.X., Song, Y., Tang, X.L., Li, Z., Wang, X.M., Wang, G.Z., Xue, Z.X., Li, X., Zhang, K., Chang, J.Q., Qiu, H.Y., 2020. Controlling factors of marine shale gas differential enrichment in southern China. Pet. Explor. Dev. 47 (3), 617–628.
Jin, S.D., Deng, H.C., Zhu, X., Liu, Y., Liu, S.B., Fu, M.Y., 2020. Orbital control on cyclical organic matter accumulation in Early Silurian Longmaxi Formation shales. Geosci. Front. 11, 533–545.
Jin, C.S., Li, C., Algeo, T.J., Planavsky, N.J., Cui, H., Yang, X., Zhao, Y., Zhang, X., Xie, S., 2016. A highly redox-heterogeneous ocean in South China during the early Cambrian (~529- 514 Ma): Implications for biota-environment co-evolution. Earth Planet. Sci. Lett. 441, 38–51.
Jin, C.S., Li, C., Peng, X.F., Cui, H., Shi, W., Zhang, Z.H., Luo, G.M., Xie, S.C., 2014. Spatiotemporal variability of ocean chemistry in the early Cambrian, South China. Sci. China Earth Sci. 57, 579–591.
Jones, B., Manning, D.A.C., 1994. Comparison of geochemical indices used for the interpretation of palaeoredox conditions in ancient mudstones. Chem. Geol. 111, 111–129.
Kodama, K.P., Hinnov, L.A., 2014. Rock Magnetic Cyclostratigraphy. New Analytical Methods in Earth and Environmental Science Series. Wiley-Blackwell, pp. 1–147.
Laskar, J., Robutel, P., Joutel, F., Gastineau, M., Correia, A.C.M., Levrard, B., 2004. A long-term numerical solution for the insolation quantities of the earth. A & A 428, 261–285.
Li, J.H., Wang, H.H., Li, W.B., Zhou, X.B., 2014. Discussion on global tectonics evolution from plate reconstruction in Phanerozoic. Acta Pet. Sin. 35 (2), 207–218 (in Chinese, English abstract).
Li, C., Cheng, M., Algeo, T.J., Xie, S.C., 2015. A theoretical prediction of chemical zonation in early oceans (> 520 Ma). Sci. China Earth Sci. 58, 1901–1909.
Li, Y.X., Montanez, I.P., Liu, Z.H., Ma, L.F., 2017. Astronomical constraints on global carbon-cycle perturbation during Oceanic Anoxic Event 2 (OAE2). Earth Planet. Sci. Lett. 462, 35–46.
Li, M.S., Kump, L.R., Hinnov, L.A., Mann, M.E., 2018. Tracking variable sedimentation rates and astronomical forcing in Phanerozoic paleoclimate proxy series with evolutionary correlation coefficients and hypothesis testing. Earth Planet. Sci. Lett. 501, 165–179.
Li, M.S., Hinnov, L., Kump, L., 2019a. Acycle: time-series analysis software for paleoclimate research and education. Comput. Geosci. 127, 12–22.
Li, M.S., Huang, C.J., Ogg, J., Zhang, Y., Hinnov, L., Wu, H.C., Chen, Z.Q., Zou, Z.Y., 2019b. Paleoclimate proxies for cyclostratigraphy: comparative analysis using a lower Triassic marine section in South China. Earth Sci. Rev. 189, 125–146.
Li, Q., Liu, G., Song, Z., Zhang, B., Sun, M., Tian, X., Yang, D., Wang, Y., Zhu, L., Cao, Y., 2022. Organic matter enrichment due to high primary productivity in the deep-water shelf: Insights from the lower Cambrian Qiongzhusi shales of the central Sichuan Basin, SW China. J. Asian Earth Sci. 239, 105417.
Liu, S., Wang, Y., Sun, W., Zhong, Y., Hong, H., Deng, B., Xia, M., Song, J., Wen, Y., Wu, J., 2016. Control of intracratonic sags on the hydrocarbon accumulations in the Marine Strata across the Sichuan Basin. J. Chengdu Univ. Technol. 43, 1–23 (in Chinese, English abstract).
Liu, Z.H., Algeo, T.J., Guo, X.S., Fan, J.X., Du, X.B., Lu, Y.C., 2017. Paleo-environmental cyclicity in the Early Silurian Yangtze Sea (South China): tectonic or glacio-eustatic control? Palaeogeogr. Palaeoclimatol. Palaeoecol. 466, 59–76.
Liu, D., Huang, C., Kemp, D.B., Li, M., Ogg, J.G., Yu, M., Foster, W.J., 2021. Paleoclimate and sea level response to orbital forcing in the Middle Triassic of the eastern Tethys. Global Planet. Change 199, 103454.
Liu, Y., Huang, C.J., Ogg, J.G., Algeo, T.J., Kemp, D.B., 2019. Oscillations of global sea-level elevation during the Paleogene correspond to 1.2-Myr amplitude modulation of orbital cycles. Earth Planet. Sci. Lett. 522, 65–78.
Liu, S.B., Jin, S.D., Liu, Y., Chen, A.Q., 2022. Astronomical forced sequence infill of Early Cambrian Qiongzhusi organic-rich shale of Sichuan Basin, South China. Sediment. Geol. 440, 106261.
Lu, Y., Jiang, S., Lu, Y., Xu, S., Shu, Y., Wang, Y., 2019. Productivity or preservation? The factors controlling the organic matter accumulation in the late Katian through Hirnantian Wufeng organic-rich shale, South China. Mar. Pet. Geol. 109, 22–35.
Lu, M., Lu, Y.H., Ikejiri, T., Sun, D., Carroll, R., Blair, E.H., Algeo, T.J., Sun, Y., 2021. Periodic oceanic euxinia and terrestrial fluxes linked to astronomical forcing during the late Devonian Frasnian-Famennian mass extinction. Earth Planet. Sci. Lett. 562, 116839.
Merdith, A.S., Collins, A.S., Williams, S.E., Pisarevsky, S., Foden, D.J., Archibald, D.B., Blades, M.L., Alessio, B.L., Armistead, S., Plavsa, D., Clark, C., Muller, D.R., 2017. A full-plate global reconstruction of the Neoproterozoic. Gondw. Res. 50, 84–134.
Meyers, S.R., Sageman, B.B., 2007. Quantification of deep-time orbital forcing by average spectral misfit. Am. J. Sci. 307, 773–792.
Myers, K.J., Wignall, P.B., 1987. Understanding Jurassic organic-rich mudrocks-new concepts using gamma-ray spectrometry and palaeoecology: examples from the Kimmeridge Clay of Dorset and the Jet Rock of Yorkshire. In: Marine Clastic Sedimentology. Springer, pp. 172–189.
Och, L.M., Shield-Zhou, G.A., Poulton, S.W., Manning, C., Thirlwall, M.F., Li, D., Chen, X., Ling, H.F., Osborn, T., Cremonese, L., 2013. Redox changes in Early Cambrian black shales at Xiaotan Section, Yunnan Province, South China. Precambr. Res. 225, 166–189.
Okada, Y., Sawaki, Y., Komiya, T., Hirata, T., Takahata, N., Sano, Y., Han, J., Maruyama, S., 2014. New chronological constraints for Cryogenian to Cambrian rocks in the Three Gorges, Weng'an and Chengjiang areas, South China. Gondwana Res. 25 (3), 1027–1044.
Pan, X.Q., 2022. Early Cambrian fossil assemblages and evolution of paleomarine environment in Jingyan-Qianwei area, southern Sichuan Province. Northwest University. PhD thesis.
Peng, C., Zou, C.C., Zhang, S.X., Wu, H.C., Lv, Q.T., Hou, H.S., Wang, C.S., 2020a. Astronomically forced variations in multiresolution resistivity logs lower Upper Cretaceous (Cenomanian-Coniacian) terrestrial formations from the Songliao Basin, northeastern China. Palaeogeogr. Palaeoclimatol. Palaeoecol. 555, 109858.
Peng, S., Babcock, L.E., Ahlberg, P., 2020b. The Cambrian Period. In: Geologic Time Scale 2020. Elsevier, pp. 565–629.
Raiswell, R., Canfield, D.E., 2012. The iron biogeochemical cycle past and present. Geochem. Perspect. 1, 1–232.
Rowe, H.D., Loucks, R.G., Ruppel, S.C., Rimmer, S.M., 2008. Mississippian Barnett Formation, Fort Worth Basin, Texas: bulk geochemical inferences and Mo-TOC constraints on the severity of hydrographic restriction. Chem. Geol. 257 (1–2), 16–25.
Sageman, B.B., Hollander, D.J., Lyons, T.W., Murphy, A.E., VerStraeten, C.A., Werne, J. P., 2003. A tale of shales: the relative roles of production, decomposition, and dilution in the accumulation of organic-rich strata, Middle-Upper Devonian, Appalachian Basin. Chem. Geol. 195, 229–273.
Sawaki, Y., Nishizawa, M., Suo, T., Komiya, T., Hirata, T., Takahata, N., Sano, Y., Han, J., Kon, Y., Maruyama, S., 2008. Internal structures and U-Pb ages of zircons from a tuff layer in the Meishucunian formation, Yunnan Province, South China. Gondwana Res. 14 (1), 148–158.
Snedden, J.W., Liu, C., 2010. A compilation of Phanerozoic sea-level change, coastal onlaps and recommended sequence designations. American Association Petroleum Geology Bulletin, 40594.
Steiner, M., Li, G.X., Qian, Y., Zhu, M.Y., Erdtmann, B., 2007. Neoproterozoic to Early Cambrian small shelly fossil assemblages and a revised biostratigraphic correlation of the Yangtze Platform (China). Palaeogeogr. Palaeogeogr. Palaeoclimatol. 254 (1–2), 67–99.
Stow, D.A.V., Huc, A.Y., Bertrand, P., 2001. Depositional processes of black shales in deep water. Mar. Pet. Geol. 18, 497–498.
Sørensen, A.L., Nielsen, A.T., Thibault, N., Zhao, Z., Schovsbo, N.H., Dahl, T.W., 2020. Astronomically forced climate change in the late Cambrian. Earth Planet. Sci. Lett. 548, 116475.
Thomson, D.J., 1982. Spectrum estimation and harmonic analysis. IEEE Process 1005–1096.
Tyson, R.V., 2001. Sedimentation rate, dilution, preservation and total organic carbon: some results of a modelling study. Org Geochem. 32, 333–339.
Waltham, D., 2015. Milankovitch period uncertainties and their impact on Cyclostratigraphy. J. Sediment. Res. 85, 990–998.
Wang, J., Li, Z.X., 2003. History of Neoproterozoic rift basins in South China: implications for Rodinia break-up. Precambr. Res. 122, 141–158.
Wang, J.G., Chen, D.Z., Wang, Q.C., Yan, D.T., Wang, Z.Z., 2007. Platform evolution and marine source rock deposition during the terminal Sinian to Early Cambrian in the Middle Yangtze region. Acta Geol. Sin. 81 (8), 1102–1109.
Wang, S.F., Zou, C.N., Dong, D.Z., Wang, Y.M., Li, X.J., Huang, J.L., Guan, Q.Z., 2015. Multiple controls on the paleoenvironment of the Early Cambrian marine black shales in the Sichuan Basin, SW China: Geochemical and organic carbon isotopic evidence. Mar. Pet. Geol. 66 (4), 660–672.
Wang, M., Chen, H., Huang, C., Kemp, D.B., Xu, T., Zhang, H., Li, M., 2020. Astronomical forcing and sedimentary noise modeling of lake-level changes in the Paleogene Dongpu Depression of North China. Earth Planet. Sci. Lett. 535, 116116 https://doi.org/10.1016/j.epsl.2020.116116.
Wang, M., Li, M., Kemp, D.B., Boulila, S., Ogg, J.G., 2022. Sedimentary noise modeling of lake-level change in the late Triassic Newark Basin of North America. Glob. Planet. Chang 208, 103706.
Weedon, G.P., 2003. Time-Series Analysis and Cyclostratigraphy. Cambridge University Press, Cambridge, UK, p. 276.
Wehausen, R., Brumsack, H., 2002. Astronomical forcing of the East Asian monsoon mirrored by the composition of Pliocene South China Sea sediments. Earth Planet. Sci. Lett. 201 (3–4), 621–636.
Wei, G.Q., Wang, D.L., Wang, X.B., Li, J., Li, Z.S., Xie, Z.Y., Cui, H.Y., Wang, Z.H., 2014. Characteristics of noble gases in the large Gaoshiti-Moxi gas field in Sichuan Basin, SW China. Pet. Expl. Dev. 41 (5), 585–590.
Xiong, M., Chen, L., Tan, X.C., Chen, X., Zheng, J., Yang, Y., Jing, C., Wang, G.X., 2023. Effects of the astronomical orbital cycle on organic matter accumulation during the Late Ordovician-early Silurian in the Upper Yangtze area, South China. J. Asian Earth Sci. 242, 105496.
Xu, H.L., Wei, G.Q., Jia, C.Z., Yang, W., Zhou, T.W., Xie, W.R., Li, C.X., Luo, B.W., 2012. Tectonica evolution of the Leshan-Longnvsi paleo-uplift and tis control on gas accumulation in the Sinian strata, Sichuan Basin. Pet. Expl. Dev. 39, 436–446.
Yan, D.T., Wang, H., Fu, Q.L., Chen, Z.H., He, J., Gao, Z., 2015. Geochemical characteristics in the Longmaxi Formation (Early Silurian) of South China: implications for organic matter accumulation. Mar. Pet. Geol. 65, 290–301.
Yang, C., 2017. High precision geochronology of the Upper Ediacaran-Lower Cambrian in South China. University of Chinese Academy of Sciences (PhD thesis) (in Chinese, English abstract).
Zhang, Z., Li, Y., Ding, G., Fan, B., Da, S., Xu, Q., Wang, Y., Chi, Z., Dong, J., Liu, C., Zhang, L., 2022a. Astronomical forcing of vegetation and climate change during the late Pliocene-early Pleistocene of the Nihewan Basin, North China. Quat. Int. 613, 1–13.
Zhang, T., Li, Y., Fan, T., Da Silva, A., Shi, J., Gao, Q., Kuang, M., Liu, W., Gao, Z., Li, M., 2022b. Orbitally-paced climate change in the early Cambrian and its implications for the history of the Solar System. Earth Planet. Sci. Lett. 583, 117420.
Zhao, J.H., Jin, Z.J., Hu, Q.H., Liu, K.Y., Liu, G.X., Gao, B., Liu, Z.B., Zhang, Y.Y., Wang, R.Y., 2019. Geological controls on the accumulation of shale gas: a case study of the early Cambrian shale in the Upper Yangtze area. Mar. Pet. Geol. 107, 426–437.

Zhao, S.Z., Li, Y., Xu, Y.J., Cheng, L., Niu, Z., Zhao, L., 2023. Earth's orbital control on organic matter enrichment in the black shales of the Wufeng-Longmaxi Formation in the Upper Yangtze Region, South China. Front. Earth Sci. 10, 938323.

Zhou, Y., Jin, S.D., Liu, Y., Liu, S.B., Zhang, Q.L., 2022. Cyclostratigraphy research on well-logging of the Lower Cambrian Qiongzhusi Formation in southwestern Sichuan Basin. Acta Sediment. Sin. https://doi.org/10.14027/j.issn.1000-0550.2022.013 (in Chinese, English abstract).

Zhou, G.X., Wei, G.Q., Hu, G.Y., Wu, S.J., Tian, Y.J., Dong, C.Y., 2020. The development setting and the organic matter enrichment of the Lower Cambrian shales from the western rift trough in Sichuan Basin. Nat. Gas Geosci. 31 (4), 498–506.

Zhu, M.Y., Babcock, L.E., Peng, S.C., 2006. Advances in Cambrian stratigraphy and paleontology: integrating correlation techniques, paleobiology, taphonomy and paleoenvironmental reconstruction. Paleobiology 15, 217–222.

Zou, C.N., Wei, G.Q., Xu, C.C., Du, J.H., Xie, Z.Y., Wang, Z.C., Hou, L.H., Yang, C., Li, J., Yang, W., 2014. Geochemistry of the Sinian-Cambrian gas system in the Sichuan Basin, China. Org Geochem. 74, 13–21.